Chin. J. Astron. Astrophys. Vol. 7 (2007), No. 5, 611–619
(*http://www.chjaa.org*)

Chinese Journal of
Astronomy and
Astrophysics

Seven-frequency VLBI Observations of the GHz-Peaked-Spectrum Source OQ 208 *

Wen-Feng Luo[1,3], Jun Yang[2,3], Lang Cui[1,3], Xiang Liu[1] and Zhi-Qiang Shen[2,4]

[1] National Astronomical Observatories / Urumqi Observatory, Chinese Academy of Sciences, Urumqi 830011; *liux@ms.xjb.ac.cn*
[2] Shanghai Astronomical Observatory, Chinese Academy of Sciences, Shanghai 200030
[3] Graduate School of Chinese Academy of Sciences, Beijing 100049
[4] Joint Institute for Galaxy and Cosmology, SHAO and USTC

Received 2006 December 22; accepted 2007 March 19

Abstract We present quasi-simultaneous VLBI images of the GHz-Peaked-Spectrum radio source OQ 208 obtained with the Very Long Baseline Array at 1.4, 1.7, 2.3, 5.0, 8.4, 15.4 GHz and the European VLBI Network at 6.7 GHz. The low frequency (1.4, 1.7 and 2.3 GHz) observations reveal a weak and extended steep-spectrum component at about 30 mas away at position angle -110°, which may be a remnant emission. The radio structure of OQ 208 consists of two mini-lobes at 5.0, 6.7, 8.4 and 15.4 GHz. Our spectral analysis further confirms that the southwest lobe undergoes free-free absorption and finds that the free-free absorption is stronger in the inner region. By fitting the 8.4 GHz images from 1994 to 2005, we obtain a separation speed of 0.031 ± 0.006 mas yr^{-1} between the two mini-lobes. This indicates a jet proper motion of $0.105\pm0.020\,c$ and a kinematic age of 219 ± 42 yr for the radio source.

Key words: galaxies: individual (OQ 208) — radio continuum: galaxies

1 INTRODUCTION

GHz-peaked-spectrum (GPS) sources, a sub-class of powerful radio sources ($L_{\rm radio} \approx 10^{45}$ erg s^{-1}), lie in the Narrow Line Region with characteristics of a steep rising spectrum at low frequencies. Synchrotron self-absorption (SSA) or free-free absorption (FFA) has been proposed for the inverted spectra (O'Dea 1998). Both mechanisms are supported by some observations (e.g. Yang et al. 2005). The previous VLBI observations indicate that most of GPS galaxies exhibit either a compact double (CD) or a compact symmetric object (CSO) morphology (e.g. Stanghellini et al. 2001).

The radio source OQ 208 (B1404+286, J1407+2827; J2000.0: $14^{\rm h}7^{\rm m}0.394 + 28^{\rm d}27'14.69''$), is one of the closest (z = 0.077) GPS sources with a spectral peak at 4.9 GHz (Dallacasa et al. 2000). It was not resolved with the Very Large Array (VLA). VLBI observations (Fey et al. 1996; Stanghellini et al. 1997) revealed double mini-lobes separated by ~ 7 mas in the NE-SW direction. Based on the multi-epoch VLBA observations at 2.3/8.4 GHz, Stanghellini et al. (1997, 2000) identified OQ 208 as a CSO, and determined a separation speed of 0.033 ± 0.013 mas yr^{-1} between the two lobes and a kinematic age of 204 ± 81 yr.

The host galaxy of OQ 208 has a rather bright core ($m_r = 14.6$) and broad recombination lines, and is classified as a Seyfert 1 galaxy (de Grijp et al. 1992) or a broad line radio galaxy (Marziani et al. 1993). The optical image displays a low-brightness tail in the direction north by east, which indicates the presence of companions in the galactic envelope (Stanghellini et al. 1993). The X-ray observation (Guainazzi et al. 2004) revealed that OQ 208 is a Compton-thick active galactic nucleus (AGN).

* Supported by the National Natural Science Foundation of China.

The compactness of OQ 208 and its proximity to us make it a good candidate for the studies of absorption mechanisms, proper motions of jet components, and the evolution of this class of sources with high-resolution VLBI observation.

In this paper, we present results of a quasi-simultaneous VLBI observation at seven frequencies (1.4, 1.7, 2.3, 5.0, 6.7, 8.4 and 15.4 GHz). A new weak component at ~ 30 mas at position angle -110° was detected and multi-frequency radio images and components' spectra were obtained. The proper motion between the two mini-lobes was estimated based on our and previous 8.4 GHz VLBI data. We adopt the cosmological model with $H_0 = 70\,\mathrm{km\ s^{-1}\ Mpc^{-1}}$, $\Omega_m = 0.3$, $\Omega_\Lambda = 0.7$ and define $S_\nu \propto \nu^\alpha$ throughout the paper.

2 OBSERVATIONS AND DATA REDUCTION

Table 1 lists some basic information of the VLBI observations. In the observations, the radio source OQ 208 was used as a fringe finder. Our VLBI observations (BY0020) were carried out at 1.7, 2.3/8.4, 5.0 and 15.4 GHz with the Very Long Baseline Array (VLBA) on 2005 May 3, for four scans at 1.7 and 5.0 GHz, and six scans at 2.3/8.4 and 15.4 GHz. Each scan lasted 4 minutes. Such repeated snap-shot mode of multiple-scans gives a good uv-coverage. The observations were made using the left circular polarization, in four 8-MHz channels and with 2 bit sampling. The data were correlated at Socorro with 2-second integration time, for 16 channels and with uniform weight.

Table 1 Parameters of the observations and of the images in Fig. 1. Col. (1), panel serial number of Fig. 1. Col. (2), observing frequency in GHz. Col. (3), observation date. Col. (4), observing array. Col. (5), recording rate in Mbps. Col. (6), program ID. Col. (7), peak flux density in mJy beam^{-1}. Col. (8), the lowest contour level (3σ) in mJy beam^{-1}. Col. (9–11), size and position angle of the restoring beam in mas and degree.

	Freq. (GHz)	Date	Array	Rate Mbps	Program ID	$S_{\rm peak}$ (mJy b^{-1})	L.C. (mJy b^{-1})	Maj. (mas)	Min. (mas)	P.A. ($^\circ$)
a	1.438	May 1, 2005	VLBA	256	BW0080	714.7	1.3	16.10	5.66	8.09
b	1.667	May 3, 2005	VLBA	128	BY0020	926.6	2.1	8.24	4.42	5.94
c	2.270	May 3, 2005	VLBA	128	BY0020	1290.1	1.0	9.81	8.94	42.30
d	2.270	May 3, 2005	VLBA	128	BY0020	1147.4	3.6	5.19	3.48	−3.06
e	4.987	May 3, 2005	VLBA	128	BY0020	1524.9	3.8	2.53	1.33	−1.30
f	6.668	Nov. 11, 2004	EVN	256	EN003B	978.1	11.7	5.88	0.67	77.80
g	8.420	May 3, 2005	VLBA	128	BY0020	985.7	3.2	1.31	0.96	1.18
h	15.365	May 3, 2005	VLBA	128	BY0020	346.3	2.0	0.80	0.54	0.75

The data at 1.4 and 6.7 GHz were analyzed in order to obtain a better spectral coverage. The 1.4-GHz data were provided by Wrobel who observed OQ 208 with an 11-minute scan and 256 Mbps recording rate with the VLBA. The 6.7-GHz data are from the EVN data archive (PI: Bartkiewicz). The EVN array consists of nine stations (Cm, Jb, Ef, Mc, On, Tr, Nt, Hh and Wb). In this observation, OQ 208 was observed for 13 minutes.

The $a\text{-}priori$ calibrations were done with the NRAO Astronomical Imaging Processing Software (AIPS) package (Cotton 1995). At each frequency, the amplitude calibration was performed using the system temperature measurements and antenna gain, the phase solutions were derived using the global fringe fitting with a 2-minute solution interval and a point-source model. After checking the solutions, we applied the solutions to the data, averaged all the channels in each IF and split the multi-source data into the single source data.

The self-calibration and imaging process were performed using the DIFMAP package (Shepherd et al. 1994). The overall amplitude self-calibration was not performed until the clean models had an amplitude close or equal to that of the short-baseline visibility. The gain correction for each antenna is a small factor (within 1 ± 0.15). We also fitted the calibrated visibility data to Gaussian models using the MODELFIT program. The approximate errors of the integrated flux density and position were calculated using the formula given by Lobanov[1]. The model-fitting results are reported in Table 2.

[1] *http://www.radionet-eu.org/wikiattach /SchoolOrganisationPages/attachments/lobanov.pdf*

Table 2 Gaussian components fitted with MODELFIT in the Difmap package. Col. (1), name of component(s). Col. (2), flux density of component in mJy. Cols. (3–4), distance and position angle with respect to component A (or A+B+C at low frequencies). Cols. (5–7), major and minor axes and position angle (P. A.) of component.

Component	Flux	Relative Position		Size of Gaussian component		
		Radius	Θ	Major	Minor	P. A.
	(mJy)	(mas)	($^\circ$)	(mas)	(mas)	($^\circ$)
	$\nu = 1.438$ GHz					
A+B+C	777.2 ± 67.8	0.00	—	1.98	1.39	-74.05
E+F	9.1 ± 3.0	8.24 ± 0.21	-134.19 ± 1.46	< 1	< 1	—
G	23.6 ± 8.0	39.38 ± 2.25	-109.70 ± 3.27	19.36	19.36	—
	$\nu = 1.667$ GHz					
A+B+C	1010.3 ± 90.0	0.00	—	2.20	1.64	0.33
E+F	11.4 ± 4.0	8.89 ± 0.12	-129.67 ± 0.80	2.35	2.35	—
G	24.5 ± 10.5	32.10 ± 1.83	-107.63 ± 3.27	13.70	13.70	—
	$\nu = 2.270$ GHz					
A+B+C	1346.1 ± 124.4	0.00	—	2.08	1.56	-8.65
E+F	66.0 ± 13.9	7.39 ± 0.37	-126.85 ± 2.87	0.79	0.79	—
G	11.5 ± 3.2	33.32 ± 4.79	-106.64 ± 8.19	11.40	11.40	—
	$\nu = 4.987$ GHz					
A	1320.0 ± 122.6	0.00	—	0.74	0.48	-57.68
B	551.9 ± 62.9	1.08 ± 0.09	-21.28 ± 4.97	1.36	0.94	17.90
C	258.8 ± 35.0	1.22 ± 0.11	-167.18 ± 5.14	0.73	0.73	—
E	95.2 ± 17.4	6.63 ± 0.15	-128.91 ± 1.28	0.24	0.24	—
F	116.9 ± 21.4	7.50 ± 0.17	-119.49 ± 1.26	0.65	0.65	—
	$\nu = 6.668$ GHz					
A+B+C	1979.7 ± 206.2	0.00	—	1.44	0.60	-3.46
E+F	139.7 ± 34.8	6.78 ± 0.50	-129.20 ± 4.19	1.34	0.35	-72.47
	$\nu = 8.420$ GHz					
A	1046.9 ± 97.4	0.00	—	0.68	0.31	-49.07
B	317.4 ± 45.5	0.92 ± 0.10	-26.76 ± 5.95	1.32	0.89	-14.40
C	280.9 ± 35.4	1.00 ± 0.05	-146.91 ± 3.09	0.60	0.33	8.45
E	84.9 ± 17.1	6.78 ± 0.11	-127.04 ± 0.88	0.61	0.53	-5.36
F	57.7 ± 15.5	7.69 ± 0.17	-117.68 ± 1.25	0.85	0.80	-85.70
	$\nu = 15.366$ GHz					
A	546.3 ± 56.4	0.00	—	0.57	0.40	-52.80
B	39.7 ± 8.1	1.27 ± 0.07	-29.28 ± 3.12	0.69	0.37	33.08
C	124.4 ± 17.3	1.18 ± 0.04	-145.63 ± 1.82	0.33	0.24	9.96
E	38.3 ± 10.5	6.79 ± 0.11	-126.76 ± 0.93	0.58	0.48	-79.03
F	16.7 ± 6.9	7.64 ± 0.22	-117.49 ± 1.62	0.92	0.61	-27.37

3 RESULTS

3.1 Radio Morphology

The final images are displayed in Figure 1. In each image, the lowest contour level is three times the off-source rms noise level. The contour levels go up by a factor of 2 from one to the next. All the images are restored using uniform weight. The restoring beam is shown as an ellipse in the lower-left corner. The peak flux density, lowest contour level, size, and position angle of the restoring beam are listed in Table 1. The model-fitting parameters of the marked components are listed in Table 2.

Our 1.4-GHz image reveals a new component marked 'G' in Figure 1a. It is a weak and extended component located at ~ 30 mas in position angle $\sim -110^\circ$. Component G also appears in the 1.7-GHz image (Fig. 1b). It is resolved at 2.3 GHz in Figure 1d when we use the full visibility data. The consistency of its position at the three frequencies completely confirms its existence. It is restored in Figure 1c when we use the short-baseline (< 20 Mλ) data. At the higher (> 2.3 GHz) frequencies, we do not detect component G after trying the various short-baseline data and different methods of weighting. This indicates that component G is intrinsically weak. The weakness is also consistent with the extrapolation from the decreasing spectrum between 1.7 and 2.3 GHz. The radio structure of OQ 208 consists of two mini-lobes (NE and

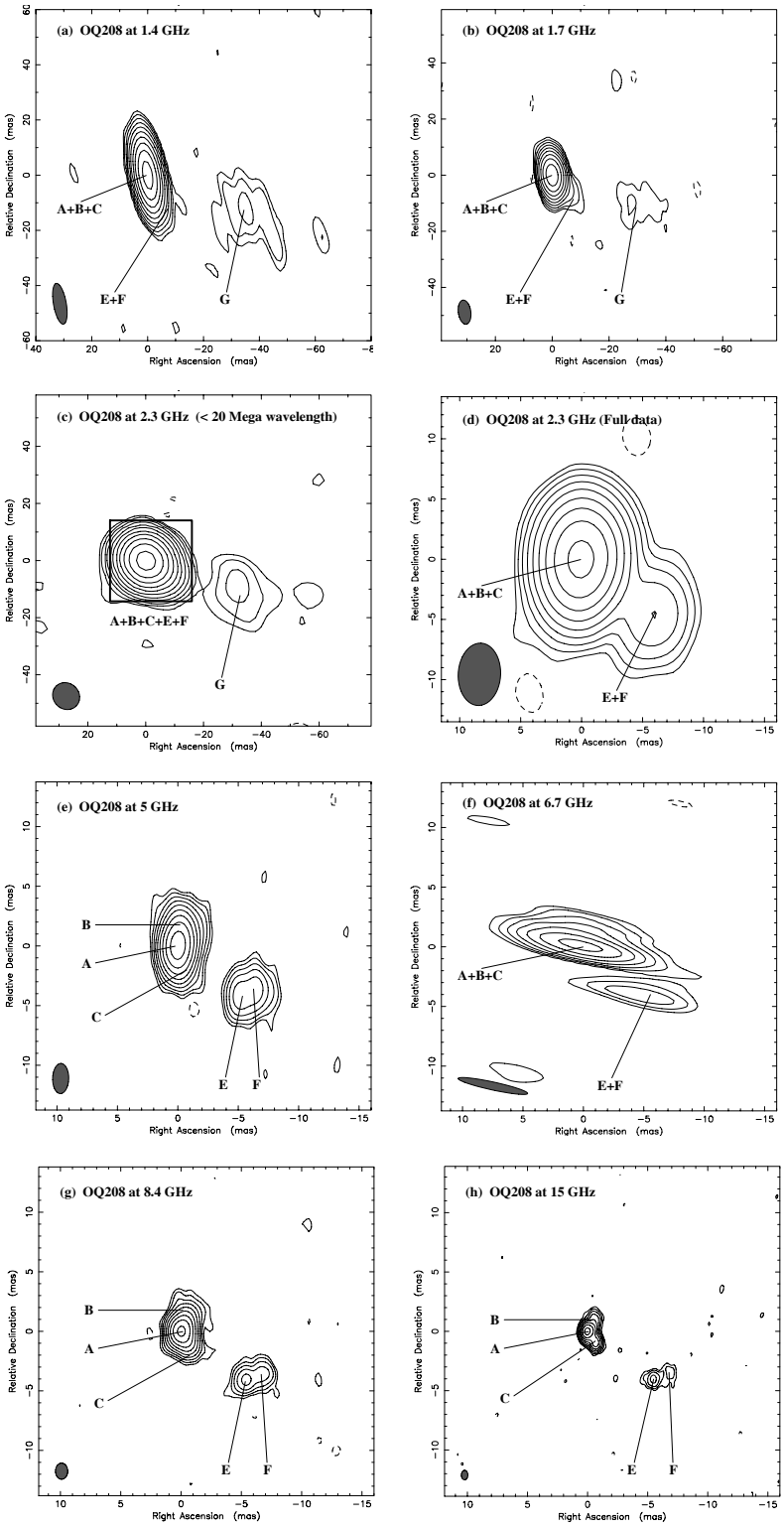

Fig. 1 Intensity images of OQ 208 from high-resolution VLBI observations at 1.4, 1.7, 2.3, 5.0, 6.7, 8.4 and 15.4 GHz. The lowest contour level is three times the off-source rms noise level. The contour levels go up by a factor of 2. The restoring beam is shown as an ellipse in the lower-left corner.

Table 3 Flux Densities of OQ 208 in the Multi-frequency VLBI Observations

Freq. (GHz)	1.438	1.667	2.270	4.987	6.668	8.420	15.365
Total (mJy)	809.9 ± 72.6	1046.2 ± 95.5	1423.6 ± 130.7	2342.8 ± 205.9	2119.4 ± 217.4	1787.8 ± 159.9	765.4 ± 73.6
NE (mJy)	777.2 ± 67.8	1010.3 ± 90.0	1346.1 ± 124.4	2130.7 ± 189.0	1979.7 ± 206.2	1645.2 ± 148.2	710.4 ± 68.9
SW (mJy)	9.1 ± 3.0	11.4 ± 4.0	66.0 ± 13.9	212.1 ± 30.1	139.7 ± 34.8	142.6 ± 24.4	55.0 ± 14.8
G (mJy)	23.6 ± 8.0	24.5 ± 10.5	11.5 ± 3.2	- - -	- - -	- - -	- - -

SW) at 2.3 and 6.7 GHz. The NE lobe can be fitted with three components (A, B and C) and the SW lobe with two components (E and F) at 5.0, 8.4 and 15 GHz. The 5.0 and 8.4 GHz images are consistent with the previous observations (e.g. Stanghellini et al. 1997; Fey et al. 1996). Kellermann et al. (1998, observed in 1995) found that there is a weak emission region including the core between the two lobes at 15 GHz. Comparing with their 15 GHz images, we did not detect any weak (> 1 mJy beam $^{-1}$) structure at 8.4 and 15.4 GHz between the two lobes although we tried different weighting methods and (u, v) taper. It is too weak and most likely that the central core region was in a relatively quiescent period at the epoch of our observations. From the VLBA 2 cm survey [2], we see that the emission from the central region was truly detected in the observations on 1995 Apr. 7, Dec. 15; 1996 Apr. 22, May 16, Oct. 27; 1997 Aug. 28; and 1998 Mar. 7, but from the observations on 1998 Oct. 30 to 2006 Apr. 28, almost nothing is found in the central region. This further confirms our results at 15.4 GHz.

The integrated flux densities of the two lobes, of component G and of the whole source at each frequency, are summarized in Table 3, together with their (generally within 10%) errors. Comparing the literature (Stanghellini et al. 1997, 2005) and our data, we can see the total flux densities of OQ 208 at 1.4 and 1.7 GHz have been stable since 1980. Our VLBI flux density at 2.3 GHz is 86% of the result observed with the telescope RATAN 600 at the same frequency (Stanghellini et al. 1998), indicating a small decrease. At 5.0 GHz, the total flux density of OQ 208 observed with VLA by Dallacasa et al. (2000) decreased by about 10% from the observation of Stanghellini et al. (1998). Compared to the VLBI observation by Stanghellini et al. (1997), our flux density of the NE lobe has decreased by 9%, while the SW lobe has been stable. We note that the total flux densities of OQ 208 observed with VLA are stable within 5% from Stanghellini et al. (1998) to Tinti et al. (2005) at 8.4 GHz. The same is true of the NE and SW lobes when we compare the VLBI data of Fey et al. (1996) with ours.

The total flux density of OQ 208 observed with VLA at 15.4 GHz is 1302 mJy (Dallacasa et al. 2000) and 1139 mJy (observed in 2002, Tinti et al. 2005). We have plotted the VLBA total flux densities of OQ 208 at 15.4 GHz from the VLBA 2 cm survey in Figure 2. From the figure, we find that its VLBA flux density is decreasing from the epoch 1999.55. This may result from the fading of the core since that time as we noted. Moreover, we find the flux density of the NE lobe decreased by 37% (reprocessed by us) from May 5, 2001 to Apr. 28, 2006, while the SW lobe remained stable. This also accounts for the drop of the VLBA total flux density of OQ 208 at 15.4 GHz.

We think that the core of OQ 208 was flaring in 1995–1996, or earlier, and has been gradually fading out since. The fading of the NE lobe at 15.4 GHz is likely due to less energy supply from the relatively quiescent central engine in recent years. On this explanation, a drop of the flux densities of OQ 208 at the lower frequencies should be expected to occur with some time delay.

3.2 Proper Motion

We also estimated the separation between components A and E over a period of about 130 months, using the available 8.4 GHz VLBI measurements. The data for epochs 1994.52, 1997.08, 1997.25, 1997.38, 1997.56, 1997.96, 1998.48, 2002.04 and 2005.33 are taken from Liu et al. (2000), Wang et al. (2003), the radio reference frame image database (RRFID) [3] and this paper. The estimate of the position errors was obtained using the standard deviation among the positions found by the different tasks, e.g. the tasks IMFIT, OMFIT, JMFIT and SLIME in AIPS, and MODELFIT in DIFMAP for the same components except ours, which have been discussed in Section 2. Typical values for the position errors are between 0.03 and 0.2 mas, depending on the size of the uv-data. We plot the separation between components A and E as a function of the observing

[2] *http://www.cv.nrao.edu/2cmsurvey/*

[3] *http://rorf.usno.navy.mil/rrfid.shtml*

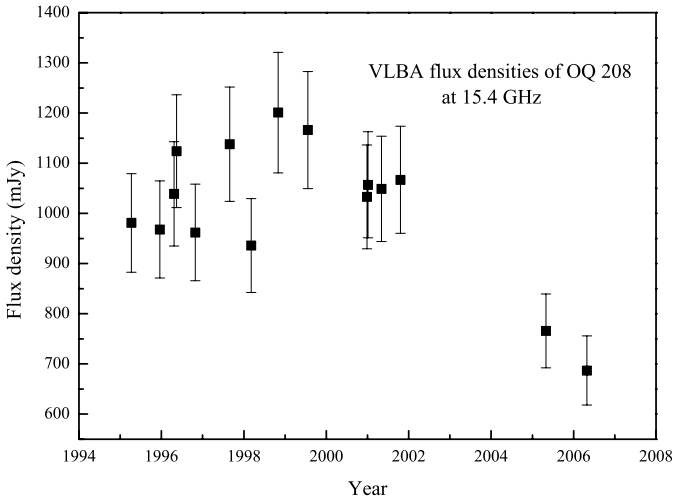

Fig. 2 VLBA total flux densities of OQ 208 at 15.4 GHz. Data are from the VLBA 2 cm survey with 10% error bars added, and the data at epoch 2005.33 are from this paper.

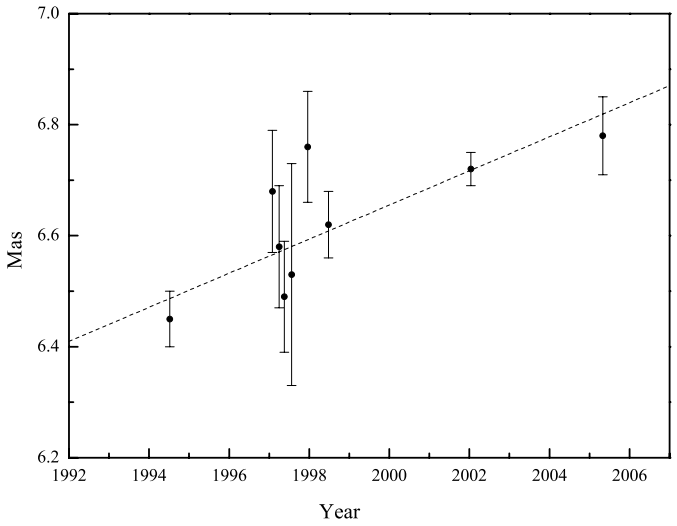

Fig. 3 Separation between components A and E in OQ 208 at 8.4 GHz.

epoch in Figure 3. A linear fit to the data gives a rate of separation. of 0.031 $\pm$0.006 mas yr $^{-1}$. This proper motion has confirmed the previous estimate of 0.033$\pm$0.013 mas yr $^{-1}$ by Stanghellini et al. (2000) with longer timescale data. The redshift of OQ 208 locates the source at a distance of $\sim$ 350 Mpc, at which 1 mas corresponds to a linear size of about 1.46 pc. Then we obtain a projected jet speed of 0.074$\pm$0.014c. Assuming an inclination of 45° between the jet and the line of sight (Stanghellini et al. 1997), we then obtain the actual jet velocity of 0.105$\pm$0.020c and hence a kinematic age of 219$\pm$42 yr for the radio source.

We also used the data from the VLBA 2 cm survey on April 7, 1995 and ours at 15.4 GHz to estimate the separation of components A and E. The result is 0.028$\pm$0.012 mas yr $^{-1}$. Both results at 8.4 and 15.4 GHz indicate that OQ 208 is indeed undergoing an expansion.

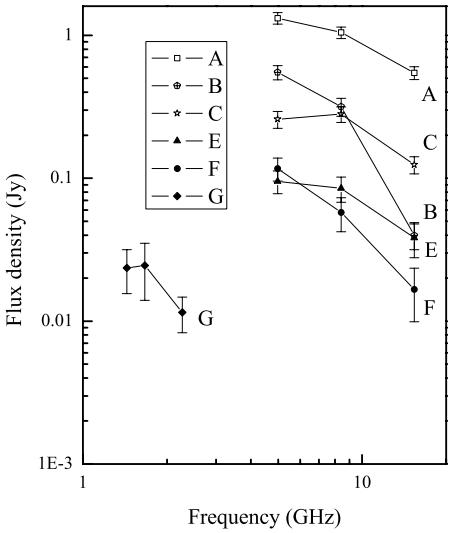

Fig. 4 Spectra of components A, B, C, E, F and G in OQ 208.

4 DISCUSSION

4.1 Property of Component G

In the images at 1.4, 1.7 and 2.3 GHz (Fig. 1), component 'G' is far from the major components. It is difficult to explain the component G in the CSO scenario. Component G could be a remnant emission from a previous radio burst, and OQ 208 may be a recurrent radio source. The steep spectral index ($\alpha = -2.4$) between 1.7 and 2.3 GHz further supports the remnant explanation for its emission losses (Marecki et al. 2003). Assuming a similar proper motion in the recurrent scenario, we could estimate that the age of component G is at least 1000 yr, which is much older than the CSO age of ~ 220 yr.

With the same resolution, the flux densities of the component G are $S_{2.3\,\mathrm{GHz}}$ = 11.5 mJy, $S_{1.7\,\mathrm{GHz}} = 24.5$ mJy and $S_{1.4\,\mathrm{GHz}}$ = 23.6 mJy. It has an inverted spectrum with a turnover frequency of ≤ 1.7 GHz, lower than for the other components. See Figure 4. If the turnover of G is mainly caused by SSA, then the turnover frequency in a homogenous, incoherent synchrotron radio source with a power-law electron energy distribution is given by Kellermann & Pauliny-Toth (1981) as

$$\nu_{\mathrm{t}} \approx 8 B^{1/5} S_{\mathrm{t}}^{2/5} \theta^{-4/5} (1+z)^{1/5} \quad \mathrm{GHz}\,, \tag{1}$$

where B is the magnetic field in Gauss, S_{t} the flux density at the peak in Jy, θ the angular size in mas and z the redshift. If we take $\nu_{\mathrm{t}} = 1.7$ GHz, $S_{\mathrm{t}} = 0.02$ Jy and $\theta = 13.7$ mas, then the estimated magnetic field is $B \sim 3.5 \times 10^4$ Gauss, too large to be real. This estimate indicates that SSA is effective at frequencies > 1.4 GHz. Therefore, FFA could be responsible for the spectral turnover.

4.2 Absorption Mechanisms

It can be estimated from Table 3 that the two lobes in OQ 208 are highly asymmetric with a flux density ratio between the north-east (NE) lobe and south-west (SW) lobe of 85±21 and 89±23 at 1.4−1.7 GHz, much larger than the ratios of 20±2, 10±1, 14±2, 12±1 and 13±2 at frequencies 2.3, 5.0, 6.7, 8.4 and 15.4 GHz, respectively. The mechanism of asymmetric free-free absorption has been used to interpret the large flux density ratio between NE and SW lobes (Kameno et al. 2000). Considering the radio photons from the receding lobe is more scattered than those from the approaching lobe, Thomson scattering was also introduced to the flux density ratio of OQ 208, but it only contributes a factor of 1.7 for the ratio (Liu et al. 2003). Xie et al. (2005) introduced the Doppler effect into the fit to the observed spectra, and found that two models, i.e. the FFA+beaming model and the SSA+beaming model, can fit the spectrum of the NE

lobe equally well. Our observations extend the spectral measurements by adding a new, low frequency of 1.4 GHz, and thus can be used to test the different models. However, it is still hard to determine which of the absorption mechanisms is the dominant one for the NE lobe. As for the SW lobe that has a turnover frequency ~ 4 GHz, SSA only is definitely not enough to account for the steep spectral index of $\alpha = 5.7$ between 1.7 and 2.3 GHz because this value is much larger than the maximum attainable spectral index ($\alpha = 2.5$) by the SSA model.

Figure 4 shows the spectra of the pc-scale components of OQ 208. The inner components A, C and E have a similar spectrum. Compared with the inner components, the outer components B and F have steeper high-frequency spectra. The flux density ratio between the counter components E and F is 2.3 at 15 GHz, 1.5 at 8.4 GHz and 0.8 at 5 GHz. The decrease at 5 GHz could be further explained by the small free-free opacity difference in the SW lobe. Using the uniform FFA-opacity model (e. g. Kameno et al. 2001), component E has a turnover frequency $\nu_{\rm t} = 5.6$ GHz and component F has $\nu_{\rm t} = 3.7$ GHz. Based on the projected distance of component G from the core, we can give a lower limit to the characteristic size of the external plasma, i.e. ~ 57 pc, which is larger than that of any components. Therefore, the uniform FFA-opacity model is effective for the two components. Both the decrease of the flux ratio and the estimated turnover frequencies agree well, indicating that component E has a higher FFA opacity than component F at the same emission frequency. Furthermore, component G has a lower turnover frequency (≤ 1.7 GHz) than components E and F. Therefore, it seems that the turnover frequency decreases from the inner component E to the outer component G. This implies that the FFA is stronger in the inner region.

4.3 Free-Free Radiation

Free-free radiation is thermal radiation, that propagates from the source through the foreground plasma, whose excitation temperature is the same as the attenuated electron temperature T_e. Spontaneous thermal radiation from the plasma is added on. Thus, the observed brightness temperature T_b can be written as

$$T_b = T_{b0} \exp(-\tau_{\rm f} \nu^{-2.1}) + T_e[1 - \exp(-\tau_{\rm f} \nu^{-2.1})] \,, \quad (2)$$

where T_{b0} is the intrinsic brightness temperature of radio source in K and $\tau_{\rm f}$ the FFA coefficient at 1 GHz. If the source is optically thin ($\nu > \nu_{\rm t}$), then $T_b \approx T_{b0}$. For OQ 208, the brightness temperature of the lobe or hot spot is $\sim 10^9$ K (e.g. Liu et al. 2002), which is much higher than the thermal temperature $T_e \sim 10^5$ K (Kameno et al. 2001). If the source is optically thick ($\nu < \nu_{\rm t}$), the second term will be close to T_e. We will expect that T_{b0} increases with decreasing frequency and is close to the inverse Compton limit $\sim 10^{12}$ K at a certain frequency if the source has a power-law spectrum with $\alpha < 0$. If we adopt $\tau_f = 8$ (Xie et al. 2005), $\exp(-\tau) \sim 3 \times 10^{-4}$ at 1 GHz and the first item is still much larger than T_e. Therefore, for our observations at frequencies greater than 1 GHz, free-free radiation can be omitted.

5 SUMMARY AND CONCLUSIONS

We present the results of some quasi-simultaneous VLBI observations of the GPS radio source OQ 208 at seven frequencies (1.4, 1.7, 2.3, 5.0, 6.7, 8.4 and 15.4 GHz). We detected a weak and extended component G at 1.4, 1.7 and 2.3 GHz, located at about 30 mas at position angle $\sim -100\,^\circ$. The component G is supposed to be a relic emission from an old radio burst and its age is estimated to be at least 1000 yr assuming a similar jet proper motion in the CSO. Though both SSA and FFA can fit the spectrum of the NE lobe well, the SW lobe must undergo FFA considering its rising spectral index of $\alpha = 5.7$ between 1.7 and 2.3 GHz, larger than the maximum attainable spectral index (2.5) for SSA. FFA is stronger in the inner region than in the outer region.

We estimate a separation speed of 0.031 ± 0.006 mas yr^{-1} between components A and E based on the 8.4 GHz VLBI observations at nine epochs and further estimate a kinematic age of 219 ± 42 yr for OQ 208. The proper motion ($0.105 \pm 0.020c$) of the lobe confirms the value estimated by Stanghellini et al. (2000) with longer timescale data.

Acknowledgements We thank the referee for valuable comments and J. Wrobel for providing us the 1.4 GHz VLBA data. VLBA (Very Long Baseline Array) is a facility of the National Radio Astronomy Observatory (NRAO), operated by Associated Universities, under cooperative agreement with the National Science Foundation. We thank the MOJAVE (Lister & Homan, 2005, AJ, 130, 1418) and 2cm Survey

(Kellermann et al., 2004, ApJ, 609, 539) programs. This work has made use of Radio Reference Frame Image Database of the United States Naval Observatory. The European VLBI Network is a joint facility of European, Chinese, South African and other radio astronomy institutes funded by their national research councils. Z.-Q. Shen acknowledges the support in part by the National Natural Science Foundation of China (Grant 10573029), Program of Shanghai Subject Chief Scientist (06XD14024), and the One-Hundred-Talent Program of Chinese Academy of Sciences.

References

Cotton W. D., 1995, In: J. A. Zensus, P. J. Diamond, P. J. Napier, eds., Very Long Baseline Interferometry and the VLBA. ASP Conference Series 82, p.189
de Grijp M. H. K., Keel W. C., Miley G. K. et al., 1992, A&AS, 96, 389
Dallacasa D., Stanghellini C., Centonza M. et al., 2000, A&A, 363, 887
Fey A. L., Clegg A. W., Fomalont E. B., 1996, ApJS, 105, 299
Guainazzi M., Siemiginowska A., Rodriguez-Pascual P. et al., 2004, A&A, 421, 461
Kellermann K. I., Pauliny-Toth I. I. K., 1981, ARA&A, 19, 373
Kellermann K. I., Vermeulen R. C., Zensus A. J. et al., 1998, AJ, 115, 1295
Kameno S., Horiuchi S., Shen Z.-Q. et al., 2000, PASJ, 52, 209
Kameno S., PhD Thesis, 2001
Liu X., Stanghellini C., Dallacasa D. et al., 2000, Chin. Phys. Lett., 17(4), 307
Liu X., Stanghellini C., Dallacasa D. et al., 2002, A&A, 385, 768
Liu X., Yang J., 2003, AcASn, 44, 296
Marziani P., Sulentic J. W., Calvani M. et al., 1993, ApJ, 410, 56
Marecki A., Barthel P. D., Polatidis A. et al., 2003, PASA, 20, 16
O'Dea C. P., 1998, PASP, 110, 493
Stanghellini C., Baum S. A., O'Dea C. P. et al., 1993, ApJ, 88, 1
Stanghellini C., Bondi M., Dallacasa D. et al., 1997, A&A, 318, 376
Stanghellini C., O'Dea C. P., Dallacasa D. et al., 1998, A&A, 131, 303
Stanghellini C., Bondi M., Dallacasa D. et al., 2000, In: Conway J. E., Polatidis A. G. et al., eds., EVN 5th Symp., Goteborg: Chalmers Technical University, p.99
Stanghellini C., Dallacasa D., O'Dea C. P. et al., 2001, A&A, 377, 377
Stanghellini C., O'Dea C. P., Dallacasa D. et al., 2005, A&A, 891, 902
Shepherd M. C., Pearson T. J., Taylor G. B., 1994, BAAS, 26, 987
Tinti S., Dallacasa D., de Zotti G. et al., 2005, A&A, 432, 31
Wang W. H., Hong X. Y., An T., 2003, Chin. J. Astron. Astrophys. (ChJAA), 3, 505
Xie G. Y., Jiang D. R., Shen Z. -Q., 2005, ApJ, 621, L13
Yang J., Liu X., Shen Z. -Q. 2005, Chin. J. Astron. Astrophys. (ChJAA), 5, 563